

## RESEARCH PAPER

# Monitoring kidney size to interpret MRI-based assessment of renal oxygenation in acute pathophysiological scenarios

Kathleen Cantow<sup>1</sup> | Thomas Gladytz<sup>2</sup> | Jason M. Millward<sup>2,3</sup> | Sonia Waiczies<sup>2,3</sup> | Thoralf Niendorf<sup>2,3</sup>  | Erdmann Seeliger<sup>1</sup> 

<sup>1</sup>Institute of Translational Physiology, Charité – Universitätsmedizin Berlin, Berlin, Germany

<sup>2</sup>Berlin Ultrahigh Field Facility (B.U.F.F.), Max Delbrück Center for Molecular Medicine in the Helmholtz Association, Berlin, Germany

<sup>3</sup>Experimental and Clinical Research Center, a joint cooperation between the Charité Medical Faculty and the Max Delbrück Center for Molecular Medicine in the Helmholtz Association, Berlin, Germany

## Correspondence

Erdmann Seeliger, Charité – Universitätsmedizin Berlin, Institut für Translationale Physiologie, Charitéplatz 1 10117 Berlin, Germany.  
Email: [erdmann.seeliger@charite.de](mailto:erdmann.seeliger@charite.de)

## Funding information

Deutsche Forschungsgemeinschaft, Grant/Award Number: CRC1365

## Abstract

**Aim:** Tissue hypoxia is an early key feature of acute kidney injury. Assessment of renal oxygenation using magnetic resonance imaging (MRI) markers  $T_2$  and  $T_2^*$  enables insights into renal pathophysiology. This assessment can be confounded by changes in the blood and tubular volume fractions, occurring upon pathological insults. These changes are mirrored by changes in kidney size (KS). Here, we used dynamic MRI to monitor KS for physiological interpretation of  $T_2^*$  and  $T_2$  changes in acute pathophysiological scenarios.

**Methods:** KS was determined from  $T_2^*$ ,  $T_2$  mapping in rats. Six interventions that acutely alter renal tissue oxygenation were performed directly within the scanner, including interventions that change the blood and/or tubular volume. A biophysical model was used to estimate changes in  $O_2$  saturation of hemoglobin from changes in  $T_2^*$  and KS.

**Results:** Upon aortic occlusion KS decreased; this correlated with a decrease in  $T_2^*$ ,  $T_2$ . Upon renal vein occlusion KS increased; this negatively correlated with a decrease in  $T_2^*$ ,  $T_2$ . Upon simultaneous occlusion of both vessels KS remained unchanged; there was no correlation with decreased  $T_2^*$ ,  $T_2$ . Hypoxemia induced mild reductions in KS and  $T_2^*$ ,  $T_2$ . Administration of an X-ray contrast medium induced sustained KS increase, with an initial increase in  $T_2^*$ ,  $T_2$  followed by a decrease. Furosemide caused  $T_2^*$ ,  $T_2$  elevation and a minor increase in KS. Model calculations yielded physiologically plausible calibration ratios for  $T_2^*$ .

**Conclusion:** Monitoring KS allows physiological interpretation of acute renal oxygenation changes obtained by  $T_2^*$ ,  $T_2$ . KS monitoring should accompany MRI-oximetry, for new insights into renal pathophysiology and swift translation into human studies.

## KEYWORDS

acute kidney injury, BOLD-MRI, hypoxia, kidney size, renal oxygenation

Kathleen Cantow and Thomas Gladytz contributed equally.

Thoralf Niendorf and Erdmann Seeliger contributed equally.

See related editorial: Andersen U.B, 2023. There is more to the kidneys than meets the eye. *Acta Physiol. (Oxf)*. e13904.

This is an open access article under the terms of the [Creative Commons Attribution-NonCommercial-NoDerivs](https://creativecommons.org/licenses/by-nc-nd/4.0/) License, which permits use and distribution in any medium, provided the original work is properly cited, the use is non-commercial and no modifications or adaptations are made.

© 2022 The Authors. *Acta Physiologica* published by John Wiley & Sons Ltd on behalf of Scandinavian Physiological Society.

## 1 | INTRODUCTION

Current options for the treatment of acute kidney injury (AKI) are not adequate. Major obstacles include the limitations of serum creatinine-based metrics.<sup>1–7</sup> To overcome this, several alternative blood- or urine-based markers reflecting renal injury, inflammation, fibrosis, or repair have been proposed. Despite the promise, the clinical performance of these markers has been modest, and none has advanced to provide a point-of-care diagnosis for AKI.<sup>3–8</sup> In general, these markers fail to reveal early events in AKI pathophysiology, such as tissue hypoxia. Recognizing these limitations, synergistic approaches that include magnetic resonance imaging (MRI) are called for.<sup>1,3,5,9–13</sup> MRI facilitates the non-invasive assessment of several structural and functional kidney features.<sup>12–20</sup> Among these, kidney size (KS) has gained substantial interest as a marker to diagnose and stage kidney disorders since KS changes are associated with several renal pathologies.<sup>21–23</sup>

What has not been considered, however, is that KS is also crucial for the interpretation of MRI-based assessments of renal tissue oxygenation obtained by blood oxygenation level-dependent (BOLD) MRI techniques. This approach relies on the fact that deoxygenated hemoglobin (deoxyHb) is paramagnetic and, therefore, impacts the MRI relaxation times  $T_2^*$  and  $T_2$ .  $T_2^*$  and  $T_2$  decrease with increasing deoxyHb concentration.  $T_2^*$  reflects significant BOLD contributions from large veins, whereas  $T_2$ -based BOLD MRI is less sensitive to macrovessels.<sup>24,25</sup>  $T_2^*$ ,  $T_2$  provide a surrogate marker of tissue oxygenation due to their dependence on the  $O_2$  saturation of hemoglobin and its relationship to the partial pressure of  $O_2$  ( $pO_2$ ) in blood and tissue.<sup>9,19,26</sup> However,  $T_2^*$ ,  $T_2$  reflect the amount of deoxyHb per tissue volume; therefore the renal  $T_2^*$ ,  $T_2$  – tissue  $pO_2$  relationship is also dependent on the blood volume and the tubular volume fractions.<sup>9,19,27,28</sup> Because acute changes in these fractions are often accompanied by KS changes, simultaneous measurements of changes in KS and  $T_2^*$ ,  $T_2$  are essential for the accurate physiological interpretation of MR-based assessments of renal oxygenation. Since tissue hypoxia is a common early feature in the pathophysiology of AKI and progression to chronic kidney disease (CKD),<sup>29–36</sup> physiological interpretation of MR probing of oxygenation could render non-invasive MR-oximetry a vital assay for research into renal (patho-)physiology and for clinical application.

Events leading to acute renal hypoxia are often associated with KS changes. Studies emulating clinical procedures such as clamping of the suprarenal aorta or renal artery during surgery, or the low arterial target pressure during cardiopulmonary bypass, revealed KS reductions.<sup>27,37</sup> Conversely, anecdotal evidence indicates opposite effects for obstructing the renal vein, such as in partial nephrectomy or thrombus formation in renal cell

carcinoma.<sup>37,38</sup> Studies emulating administration of X-ray contrast media (CM) for cardiac procedures showed renal hypoxia and increased intratubular pressure.<sup>31,39–41</sup> Due to the relatively rigid renal capsule, the latter results in an “intrarenal compartment syndrome”: as intrarenal pressure increases, intrarenal blood vessels become compressed, leading to tissue hypoxia.<sup>4,42–44</sup> Accordingly, KS should significantly increase.

Recognizing the potential of MR-based probing of renal oxygenation as a meaningful tool for research into renal physiology and disorders, this study provides systematic tests for acute changes in  $T_2^*$  and  $T_2$  as markers of oxygenation, and in KS determined from the  $T_2^*$ ,  $T_2$  maps.<sup>37</sup> Serial in vivo parametric MRI mapping of  $T_2^*$ ,  $T_2$  was performed in rats during interventions that alter renal tissue oxygenation reversibly (a brief occlusion of the suprarenal aorta, the left renal vein or both; hypoxemia), and with longer-lasting effects (injection of CM or furosemide). We hypothesize that monitoring KS will allow physiological interpretation of acute changes in renal oxygenation measured by  $T_2^*$ ,  $T_2$ .

## 2 | RESULTS

### 2.1 | Aortic occlusion, renal venous occlusion, combined occlusion

By inflation of MR-safe remotely-controlled occluders, short-term occlusions of the suprarenal aorta, the left renal vein, and simultaneous occlusions of both vessels were performed.<sup>45–47</sup>

Upon occlusion of the suprarenal aorta, the coronal mid-slice cross-sectional area of the kidney (hereafter referred to as “kidney size,” KS) determined from  $T_2$  maps (Figure 1A) decreased by  $6 \pm 1\%$  (mean  $\pm$  SEM; Figure 1B). Upon occlusion release, KS returned to baseline. Aortic occlusion resulted in decreases in  $T_2$  in the renal cortex (CO), outer medulla (OM), and inner medulla (IM) of  $22 \pm 2\%$ ,  $27 \pm 2\%$ , and  $13 \pm 3\%$  (Figure 1C–E). Upon release,  $T_2$  in the IM initially decreased further, yet  $T_2$  in all layers quickly returned to baseline. Similar results were obtained for  $T_2^*$ . Upon aortic occlusion, KS determined from  $T_2^*$  maps decreased by  $6 \pm 2\%$  and returned to baseline upon release (Figure 1B).  $T_2^*$  changes during aortic occlusion were more pronounced than for  $T_2$ , decreasing by  $29 \pm 3\%$ ,  $39 \pm 3\%$ , and  $22 \pm 4\%$  in the CO, OM, and IM (Figure 1C–E). Upon release,  $T_2^*$  in the IM initially decreased further, yet  $T_2^*$  for all layers returned to baseline. Changes in  $T_2$  showed a strong correlation with changes in KS; correlations with changes in  $T_2^*$  were more moderate (Table 1).

Upon occlusion of the renal vein,  $T_2$ -derived KS increased by  $5 \pm 1\%$  and returned to baseline upon release (Figure 2B). Venous occlusion led to  $T_2$  decreases in all

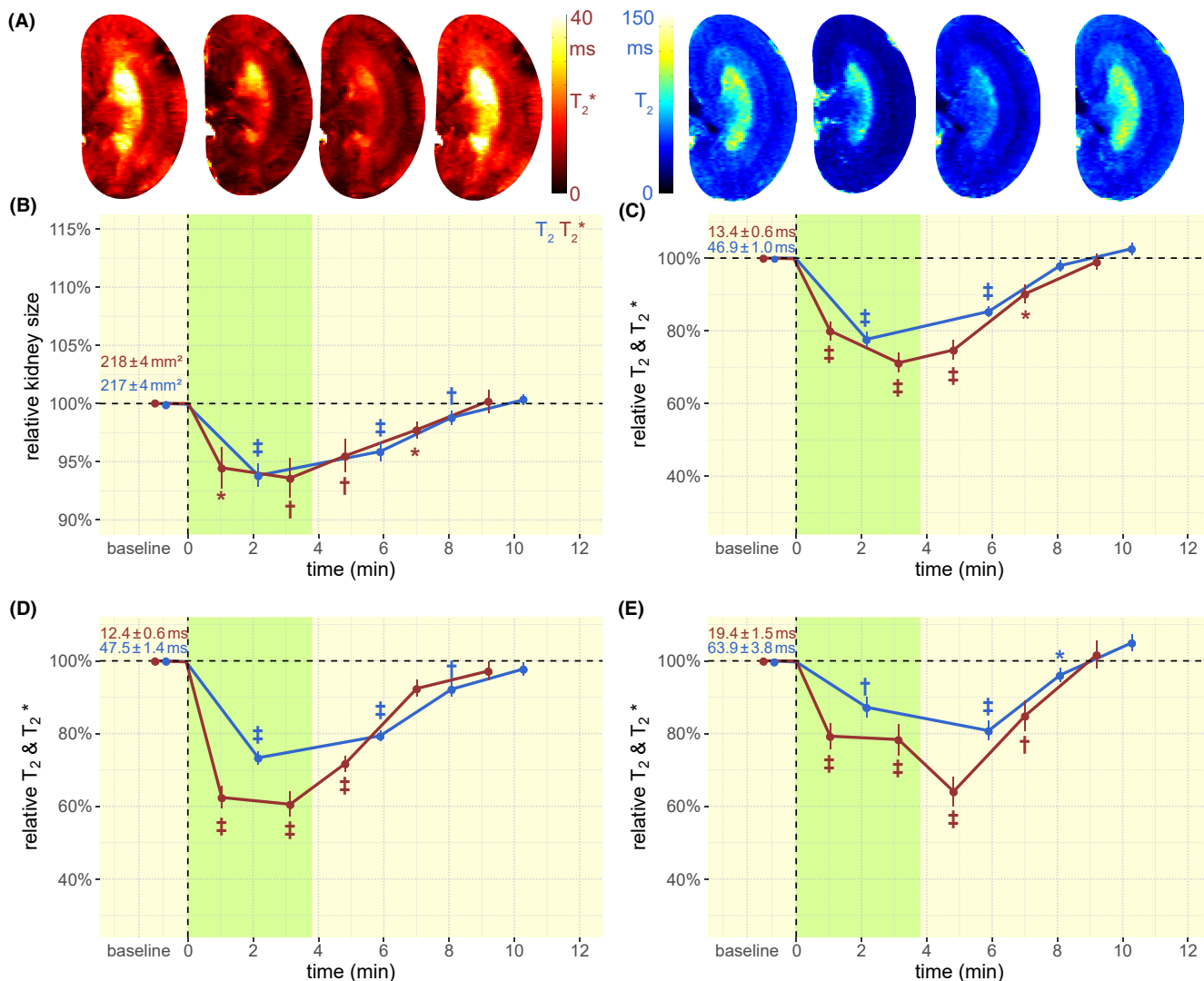


**FIGURE 1** Time courses during occlusion of the suprarenal aorta and recovery. (A) Exemplary  $T_2^*$  (left) and  $T_2$  (right) maps obtained for a rat kidney in vivo. Time course of relative changes (mean  $\pm$  SEM) for (B) kidney size (cross-sectional area) and  $T_2$  (blue) and  $T_2^*$  (red) obtained for (C) cortex (CO), (D) outer medulla (OM), and (E) inner medulla (IM) before the intervention (baseline), during the intervention (green area), and during recovery. Absolute baseline values (mean  $\pm$  SEM) are denoted; \* $p < 0.05$ ; † $p < 0.01$ ; ‡ $p < 0.001$ .

renal layers which exceeded those observed for aortic occlusion, with decreases of  $33 \pm 2\%$ ,  $39 \pm 2\%$ , and  $32 \pm 6\%$  in the CO, OM, and IM (Figure 2C–E).  $T_2^*$ -derived KS increased by  $7 \pm 1\%$  and returned to baseline upon release (Figure 2B). The  $T_2^*$  decreases in CO, OM, and IM were larger than those in  $T_2$  ( $60 \pm 3\%$ ,  $60 \pm 2\%$ , and  $58 \pm 4\%$ ; Figure 2C–E), and much larger than the  $T_2$  decreases during aortic occlusion. Restoration of  $T_2$  and  $T_2^*$  toward baseline upon release of venous occlusion occurred somewhat slower than following aortic occlusion. Changes in  $T_2$  showed moderate negative correlations with changes in KS, while negative correlations with changes in  $T_2^*$  were moderate in the CO, and weak in the OM and IM (Table 1).

Simultaneous occlusion of both the suprarenal aorta and the renal vein did not affect KS; yet there was a small drop in  $T_2^*$ -derived KS about 1 min after release of the

occlusion (Figure 3B). Simultaneous aortic and venous occlusion resulted in decreases in  $T_2$  of  $23 \pm 1\%$ ,  $28 \pm 1\%$ , and  $20 \pm 3\%$  in the CO, OM, and IM (Figure 3C–E). Changes in  $T_2^*$  were more pronounced than  $T_2$  changes, though less dramatic than those observed with venous occlusion alone, with reductions of  $46 \pm 4\%$ ,  $55 \pm 2\%$ , and  $44 \pm 4\%$  in the CO, OM, and IM (Figure 3C–E). The  $T_2$  and  $T_2^*$  return to baseline were comparable to that upon release of aortic occlusion. Changes in  $T_2$  and  $T_2^*$  did not show any significant correlation with changes in KS (Table 1).

## 2.2 | Hypoxemia

A brief period of hypoxemia was induced by lowering the inspiratory oxygen fraction ( $FiO_2$ ) from 21% (normoxia)

**TABLE 1** Repeated-measures correlation between changes in kidney size and changes in  $T_2$  and  $T_2^*$  for six clinically relevant pathophysiological scenarios

Intervention	Layer	$T_2 R_{RM}$	$T_2 R^2$	$T_2 p$ -value	$T_2^* R_{RM}$	$T_2^* R^2$	$T_2^* p$ -value
Aortic	Cortex	<b>0.81</b>	<b>0.65</b>	$2 \times 10^{-14}$	<b>0.52</b>	<b>0.27</b>	$7 \times 10^{-6}$
Occlusion	Outer medulla	<b>0.81</b>	<b>0.66</b>	$2 \times 10^{-14}$	<b>0.54</b>	<b>0.29</b>	$3 \times 10^{-6}$
	Inner medulla	<b>0.66</b>	<b>0.43</b>	$3 \times 10^{-8}$	<b>0.44</b>	<b>0.19</b>	$2 \times 10^{-4}$
Venous	Cortex	<b>-0.54</b>	<b>0.29</b>	$7 \times 10^{-6}$	<b>-0.62</b>	<b>0.39</b>	$2 \times 10^{-9}$
Occlusion	Outer medulla	<b>-0.57</b>	<b>0.32</b>	$2 \times 10^{-6}$	<b>-0.42</b>	<b>0.18</b>	$2 \times 10^{-4}$
	Inner medulla	<b>-0.55</b>	<b>0.30</b>	$5 \times 10^{-6}$	<b>-0.38</b>	<b>0.15</b>	$6 \times 10^{-4}$
Aortic-venous	Cortex	0.18	0.03	0.26	-0.02	0.00	0.87
Occlusion	Outer medulla	0.17	0.03	0.29	0.01	0.00	0.97
	Inner medulla	0.23	0.05	0.15	0.10	0.01	0.45
Hypoxemia	Cortex	<b>0.38</b>	<b>0.15</b>	$1 \times 10^{-2}$	<b>0.43</b>	<b>0.18</b>	$1 \times 10^{-3}$
	Outer medulla	<b>0.69</b>	<b>0.48</b>	$1 \times 10^{-7}$	0.19	0.04	0.15
	Inner medulla	<b>0.46</b>	<b>0.21</b>	$1 \times 10^{-3}$	0.24	0.06	0.07
Iodixanol	Cortex	<b>0.71</b>	<b>0.50</b>	$6 \times 10^{-11}$	<b>0.30</b>	<b>0.09</b>	<b>0.02</b>
	Outer medulla	<b>0.60</b>	<b>0.36</b>	$2 \times 10^{-7}$	0.10	0.01	0.45
	Inner medulla	-0.01	0.01	0.95	-0.02	0.00	0.90
Furosemide	Cortex	<b>0.79</b>	<b>0.64</b>	$2 \times 10^{-5}$	0.30	0.09	0.19
	Outer medulla	<b>0.84</b>	<b>0.71</b>	$2 \times 10^{-6}$	<b>0.50</b>	<b>0.25</b>	<b>0.02</b>
	Inner medulla	<b>0.51</b>	<b>0.26</b>	<b>0.02</b>	0.19	0.04	0.40

Note: The bold values indicate  $p < 0.05$ , the exact  $p$ -values are given in columns 5 and 8.

Abbreviations:  $R_{RM}$ , repeated measures correlation coefficient;  $R^2$ , coefficient of determination.

to 10% (hypoxia).<sup>45,48</sup> Induction of hypoxemia reduced  $T_2$ -derived KS by  $2 \pm 1\%$ , and  $T_2$  in CO, OM, and IM by  $18 \pm 3\%$ ,  $15 \pm 3\%$ , and  $8 \pm 3\%$  (Figure 4).  $T_2^*$ -derived KS was reduced by  $3 \pm 1\%$ , and  $T_2^*$  was reduced by  $23 \pm 4\%$ ,  $29 \pm 4\%$ , and  $25 \pm 5\%$  in the CO, OM, and IM.  $T_2$  changes correlated with changes in KS moderately in the OM, and weakly in the CO and IM;  $T_2^*$  changes correlated weakly only in the CO (Table 1).

### 2.3 | X-ray CM iodixanol

Bolus injection of the CM, iodixanol, into the thoracic aorta induced a sustained increase in KS, as determined from  $T_2$  and  $T_2^*$  maps, with peaks of  $10 \pm 2\%$  and  $8 \pm 2\%$  about 6 min after the injection (Figure 5B).  $T_2$  increased by  $14 \pm 3\%$  and  $17 \pm 5\%$  in the CO and OM immediately after CM injection, then normalized (Figure 5C–E). In the IM,  $T_2$  decreased by  $17 \pm 7\%$  about 17 min after CM and remained below baseline for the duration of the observation.  $T_2^*$  showed an initial increase of  $21 \pm 3\%$  and  $24 \pm 5\%$  in the CO and OM immediately after CM, then decreased below baseline levels within about 16 min. In the IM,  $T_2^*$  decreased by  $33 \pm 11\%$  by about 16 min and remained below baseline.  $T_2$  changes in the CO and OM

were strongly correlated with changes in KS;  $T_2^*$  changes in the CO showed a weak correlation (Table 1).

### 2.4 | Furosemide

Furosemide induced an increase of up to  $4 \pm 1\%$  in  $T_2$ -derived KS (Figure 6B) and increased  $T_2$  in the CO and OM by up to  $11 \pm 2\%$  and  $19 \pm 2\%$ ; changes in the IM were not significant (Figure 6C–E).  $T_2^*$ -derived KS changes did not reach statistical significance (Figure 6B).  $T_2^*$  in the CO and OM increased by up to  $6 \pm 1\%$  and  $28 \pm 4\%$ ;  $T_2^*$  changes in the IM were not significant (Figure 6C–E).  $T_2$  changes in the CO and OM showed strong correlations with changes in KS;  $T_2$  changes in the IM and  $T_2^*$  changes in the OM showed weak correlations (Table 1).

Urethane anesthesia provided stable systemic hemodynamics throughout all experiments as monitored by arterial pressure (Table S1).<sup>49</sup>

### 2.5 | Biophysical model

Using the biophysical model described in the “Methods” section, we estimated changes in  $O_2$  saturation of Hb (Sat)

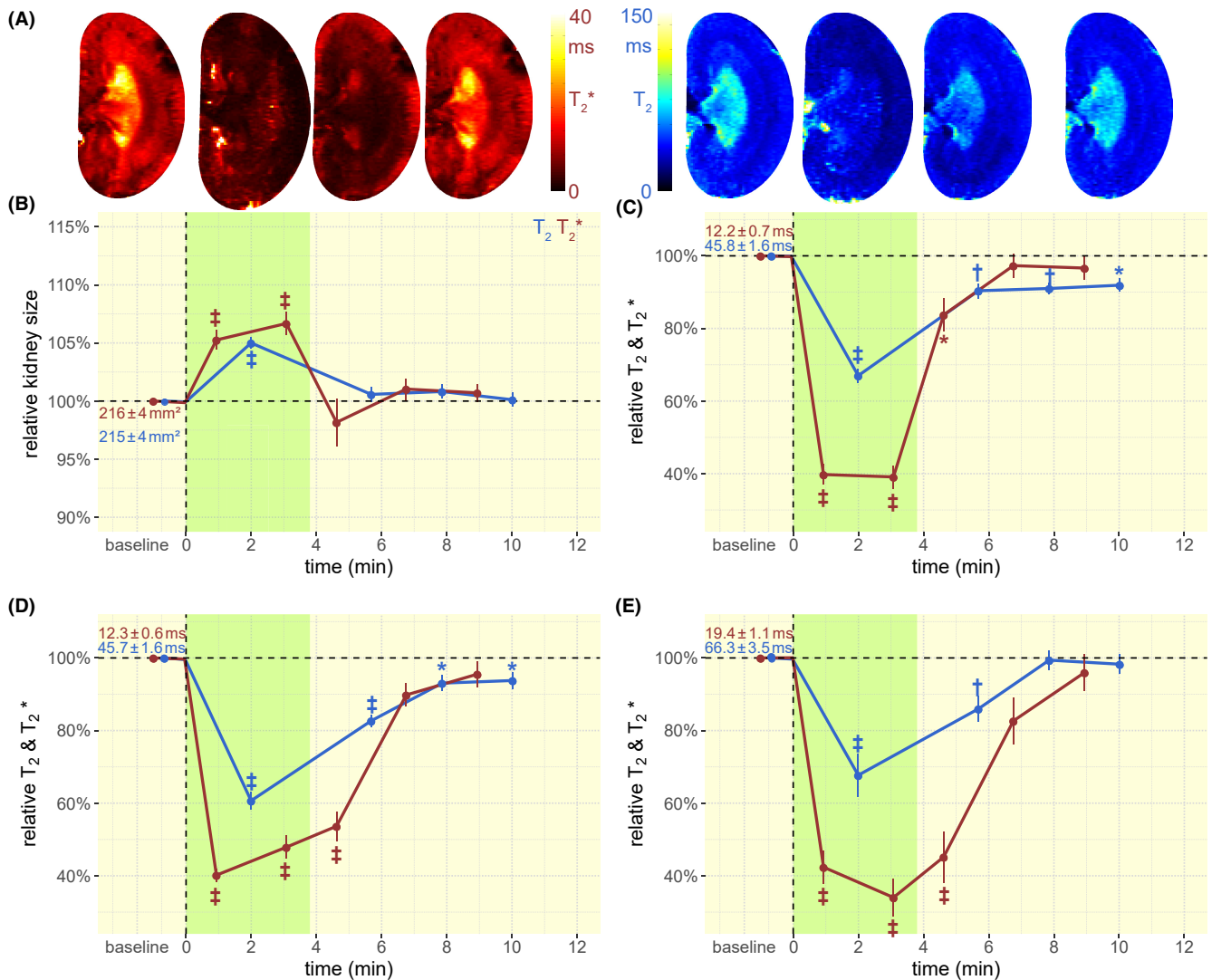


**FIGURE 2** Time courses during occlusion of the renal vein and recovery. (A) Exemplanary  $T_2, T_2^*$  maps obtained for a rat kidney in vivo. Time course of relative changes for (B) kidney size and  $T_2, T_2^*$  for (C) CO, (D) OM, and (E) IM. Colors, absolute baseline values, and significance signs as in Figure 1.

from measured changes in  $T_2^*$  and in kidney size for the three vascular occlusions. According to Equation (4) of the biophysical model, these changes are expressed by the ratio of  $(1 - \text{Sat})_{\text{occlusion}} / (1 - \text{Sat}_0)_{\text{before occlusion}}$ . The average  $(1 - \text{Sat}) / (1 - \text{Sat}_0)$  ratio in all renal layers, for all three occlusions, overall occlusion time points was approximately 2.1 (range 1.9–2.9, Table 2). On average, a relative 2.1-fold increase in the proportion of deoxyHb was found.

### 3 | DISCUSSION

Renal tissue hypoxia occurs very early in most forms of AKI and is a key feature in the progression to CKD and in diabetic kidney disease.<sup>29–36,50</sup> MRI offers non-invasive full coverage of the kidney, and the MRI relaxation times  $T_2^*$ ,  $T_2$  appear to be ideal surrogate markers of renal

oxygenation. However, the relationship between renal tissue  $pO_2$  and  $T_2^*$ ,  $T_2$  is confounded by changes in hematocrit, the  $O_2$  affinity of hemoglobin, and crucially, the blood and tubular volume fractions.<sup>9,19,27,28</sup> Here, we performed serial MR-based measurements of kidney size and  $T_2^*$ ,  $T_2$  during clinically realistic interventions in rats, directly while they were in the MR scanner, to examine this relationship. Our results demonstrate that monitoring of KS allows physiological interpretation of acute renal oxygenation changes obtained by  $T_2^*$ ,  $T_2$ .

Several surgical procedures (e.g., partial nephrectomy) require cross-clamping of the renal artery or suprarenal aorta, the renal vein, or simultaneous occlusions of both.<sup>51,52</sup> If maintained for too long, such occlusions risk renal ischemia–reperfusion injury. At the onset of occlusions, renal tissue perfusion and  $O_2$  delivery rapidly diminish, but  $O_2$  consumption by

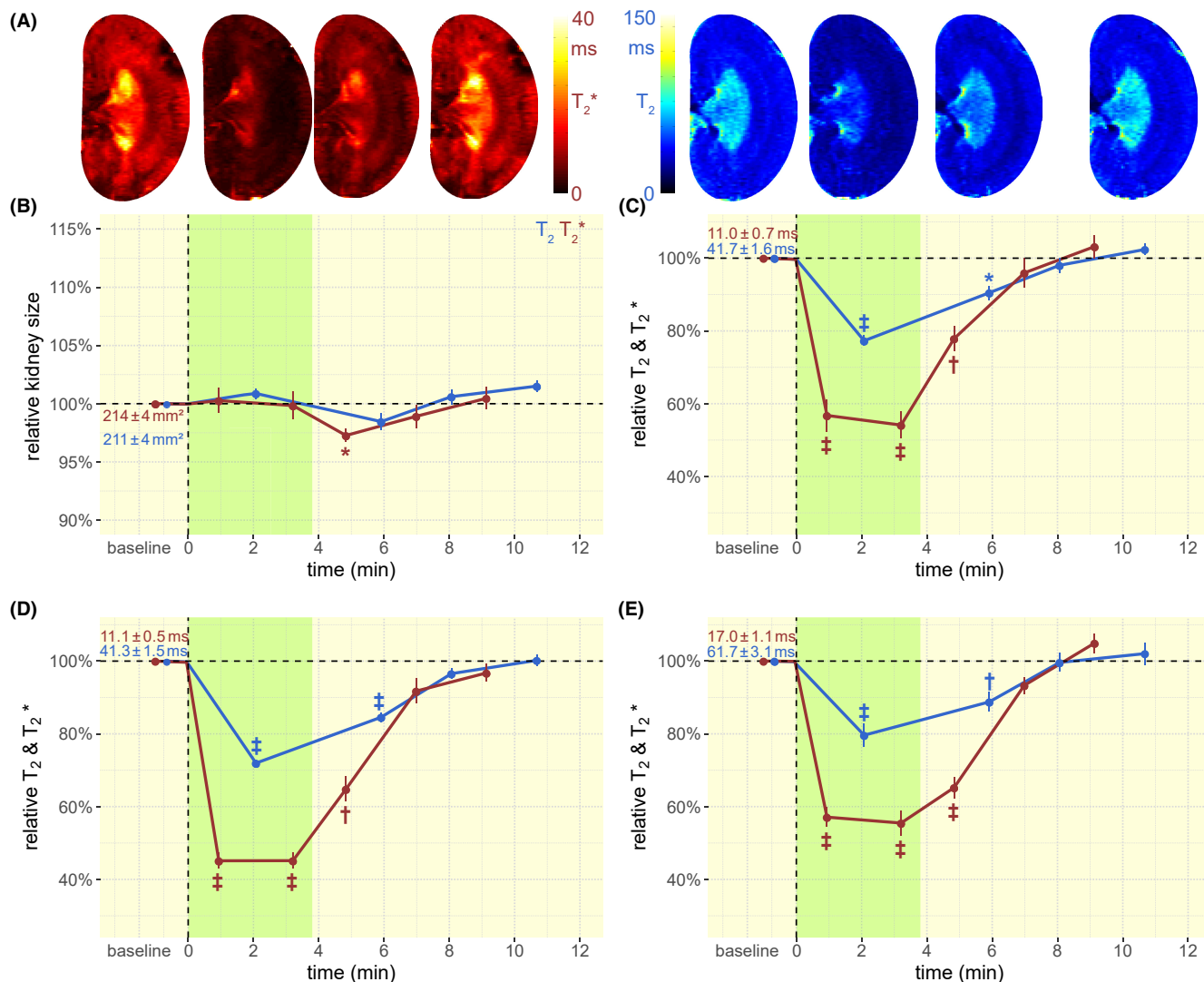


**FIGURE 3** Time courses during simultaneous occlusion of the aorta and the renal vein and recovery. (A) Exemplary  $T_2, T_2^*$  maps obtained for a rat kidney in vivo. Time course of relative changes for (B) kidney size and  $T_2, T_2^*$  for (C) CO, (D) OM, and (E) IM. Colors, absolute baseline values, and significance signs as in Figure 1.

active tubular transports continues, leading to a rapid and massive decline in tissue  $pO_2$  and  $O_2$  saturation of hemoglobin in intrarenal blood.<sup>45</sup> Our previous studies with invasive probes (the gold standard) showed an equivalent decrease in tissue  $pO_2$  and  $O_2$  saturation of hemoglobin following both venous occlusion and aortic occlusion.<sup>27,45,53</sup> However, in the present study, we observed that decreases in  $T_2^*, T_2$  following venous occlusion were much more pronounced than for aortic occlusion. The reason for this discrepancy is that the changes in  $T_2^*, T_2$  reflect changes in the blood volume fraction in response to the occlusions, that is, changes in the amount of deoxyHb per tissue volume, rather than directly mirroring  $O_2$  saturation of hemoglobin. Upon aortic occlusion, the inflow of blood into the kidney is abruptly stopped while outflow via the renal vein continues, until pressures in intrarenal vessels and the

vena cava are equalized. This reduces intrarenal blood volume and deoxyHb.<sup>45,53</sup> Conversely, upon venous occlusion, the outflow of blood is abruptly stopped, while the inflow via the renal artery continues until the distension of intrarenal vessels is counterbalanced by the resistance of the renal tissue and the relatively rigid capsule, leading to an increase in intrarenal blood volume and deoxyHb.<sup>45,53</sup> Consequently, renal oxygenation assessments by  $T_2^*, T_2$  alone will overestimate tissue hypoxia during venous occlusion and underestimate it during aortic occlusion. Simultaneous aortic and venous occlusion lowers tissue  $pO_2$  and  $O_2$  saturation of hemoglobin by a comparable degree to aortic occlusion and venous occlusion but does not change the blood volume fraction; accordingly, the decrease in  $T_2^*, T_2$  was less than for venous occlusion and more than for aortic occlusion, as illustrated qualitatively in Figure 7.

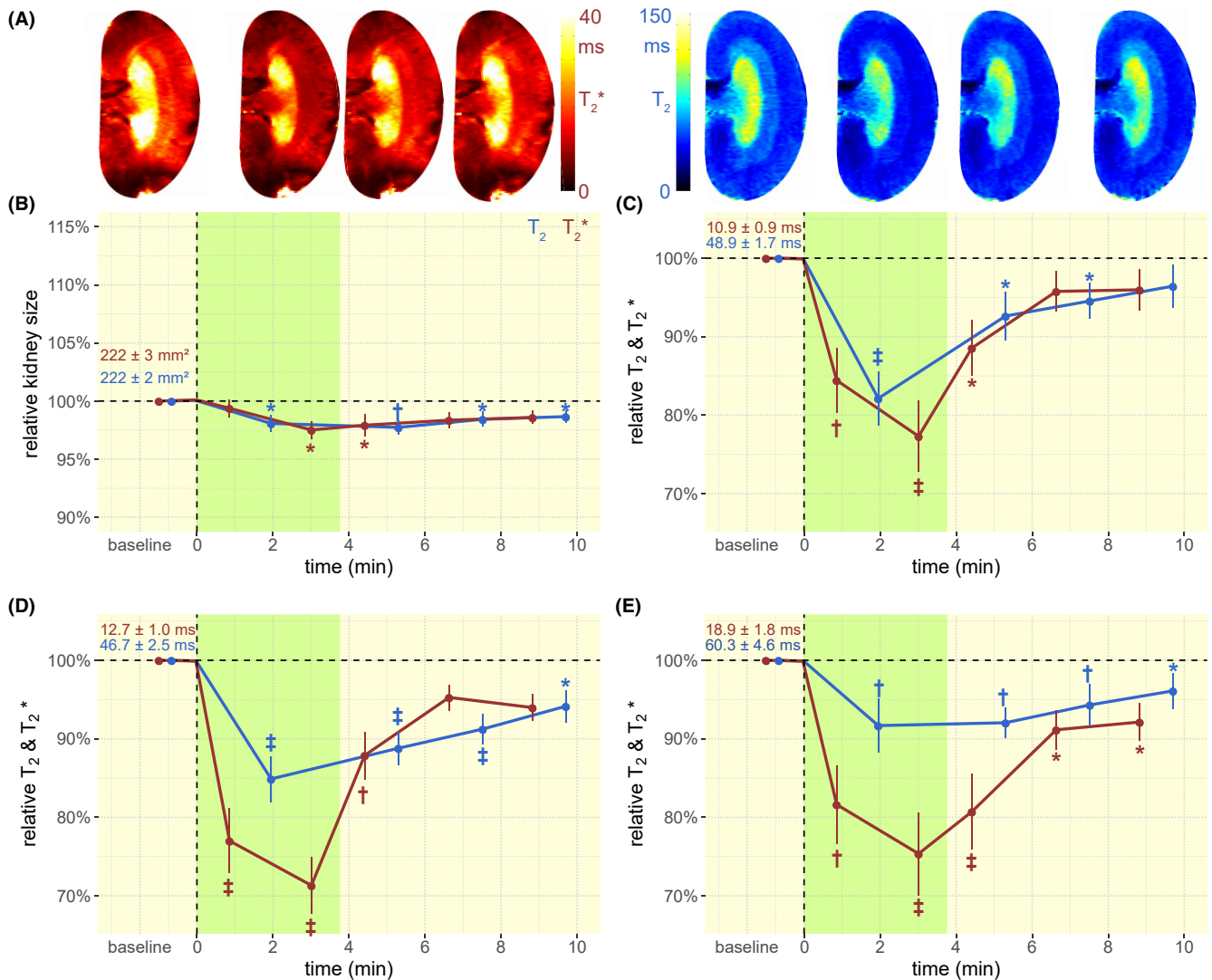


**FIGURE 4** Time courses during hypoxemia and recovery. (A) Exemplary  $T_2, T_2^*$  maps obtained for a rat kidney in vivo. Time course of relative changes for (B) kidney size and  $T_2, T_2^*$  for (C) CO, (D) OM, and (E) IM. Colors, absolute baseline values, and significance signs as in Figure 1.

Changes in renal blood volume in response to these interventions were associated with parallel changes in KS. Upon aortic occlusion, KS decreased, and this change was correlated with changes in  $T_2^*$ ,  $T_2$  in all renal layers. Conversely, upon venous occlusion, KS increased, and this was negatively correlated with changes in  $T_2^*$ ,  $T_2$ . With simultaneous aortic and venous occlusion, there was no KS change, and no correlation with  $T_2^*$ ,  $T_2$  changes (Figure 7). Thus, physiological interpretation of  $T_2^*$ ,  $T_2$  as surrogate markers for renal tissue oxygenation must take into account changes in KS. If  $T_2^*$ ,  $T_2$  decrease and KS remains unchanged, tissue oxygenation is reduced. If  $T_2^*$ ,  $T_2$  decreases, and KS also decreases, the reduction in tissue oxygenation is more severe than if KS is unchanged; if  $T_2^*$ ,  $T_2$  decreases, and KS increases, the reduction in tissue oxygenation is less severe.

Clinical scenarios with decreased hematocrit or reduced pulmonary  $O_2$  diffusion lead to arterial hypoxemia, and the risk of AKI.<sup>36,54</sup> We induced arterial hypoxemia, thus reducing renal  $O_2$  supply. The decrease in blood  $pO_2$  is attenuated by arterial chemoreceptor-actuated increase in ventilation. On the other hand, enhanced breathing reduces blood  $pCO_2$  and increases blood pH, which increases the  $O_2$  affinity of hemoglobin so that it releases less  $O_2$  in the microcirculation.<sup>45</sup> The ensuing decrease in renal tissue  $pO_2$  is milder than that during the vascular occlusions,<sup>48</sup> and the observed reduction in  $T_2^*$ ,  $T_2$  are more subtle. The  $T_2^*$ ,  $T_2$  decrease was accompanied by a KS reduction, which is related to hypoxemia-induced extra-renal vasodilation, resulting in a drop in arterial pressure and an ensuing decrease in renal arterial inflow.<sup>45,48</sup> Thus,  $T_2^*$ ,  $T_2$  and KS measurements reveal even subtle changes in renal tissue oxygenation.

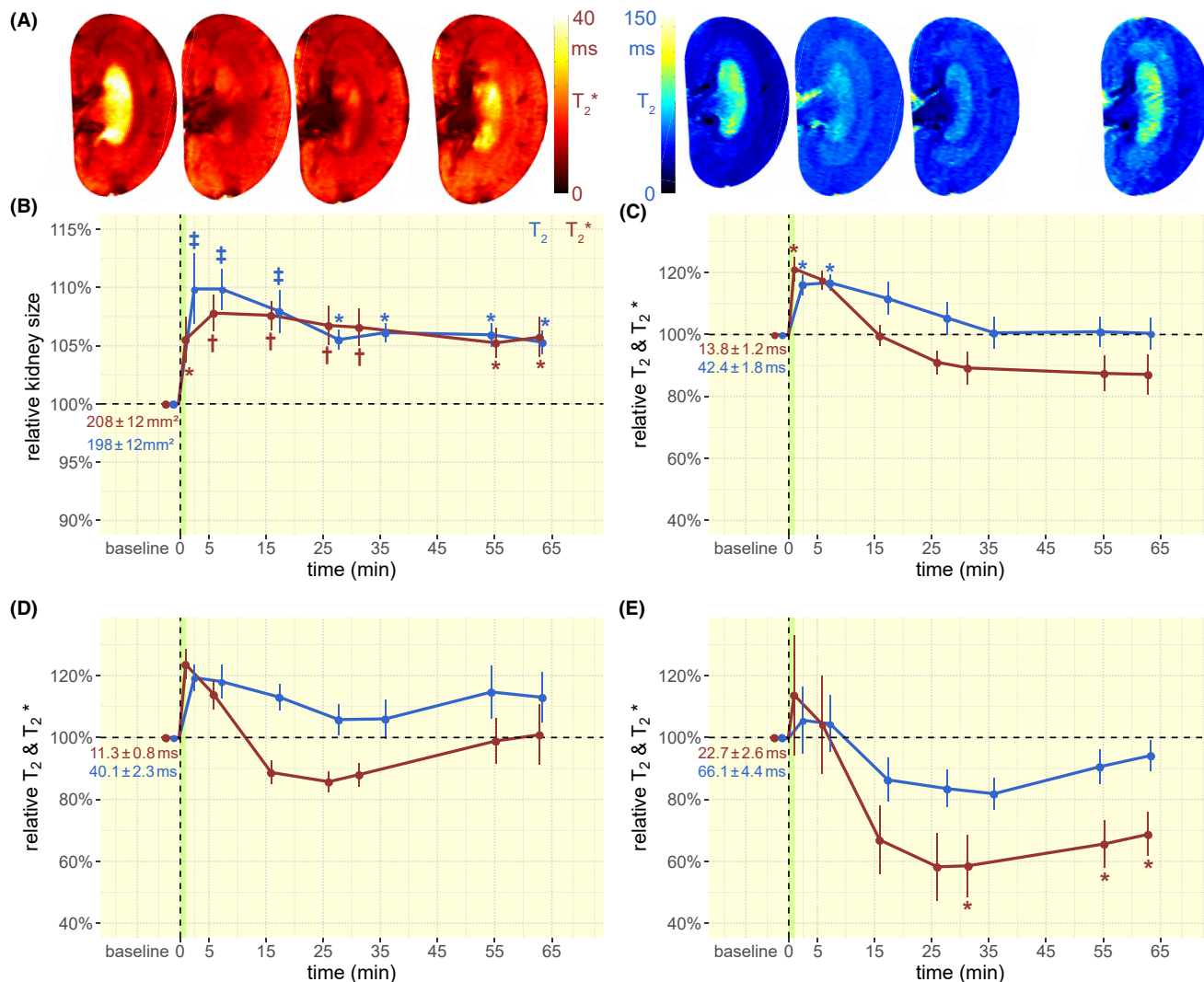


**FIGURE 5** Time courses following administration of an X-ray CM. (A) Exemplary  $T_2, T_2^*$  maps obtained for a rat kidney in vivo. Time course of relative changes for (B) kidney size and  $T_2, T_2^*$  for (C) CO, (D) OM, and (E) IM. Colors, absolute baseline values, and significance signs as in Figure 1.

X-ray CM can induce AKI, especially at large doses administered for cardiac interventions.<sup>4</sup> This is the result of several mechanisms that lead to renal hypoperfusion and hypoxia,<sup>4</sup> including fluid viscosity-induced increase in intratubular pressure,<sup>39,40,55</sup> resulting in intrarenal compartment syndrome. We observed an initial increase in  $T_2^*, T_2$  upon iodixanol injection in the CO and OM, followed by a decrease toward baseline levels for  $T_2$  and even lower levels for  $T_2^*$ . While these  $T_2^*, T_2$  changes are consistent with a previous MRI study,<sup>56</sup> they differ from results we previously obtained with invasive  $pO_2$  probes.<sup>41</sup> Using the same experimental paradigm as in the present study, we observed an immediate and massive drop in  $pO_2$  upon CM, that was sustained for 60 min.<sup>41</sup> The explanation for this apparent discrepancy becomes clear when we note that KS increased upon CM injection, peaking within 6 min, and remained enlarged throughout the observation

period. This reflects the compartment syndrome that results in compression of the intrarenal vessels and thus decreased deoxyHb (Figure 7). While the initial  $T_2^*, T_2$  increase in CO and OM appears to reflect improved tissue oxygenation, it in fact deteriorates, as demonstrated with the  $pO_2$  probes,<sup>41</sup> and indicated here by the KS change. The sustained renal enlargement indicates continued compartment syndrome, and thus the apparent return of  $T_2$  toward baseline does not in fact reflect normalization of tissue oxygenation, and the  $T_2^*$  decrease below baseline greatly underestimates the degree of hypoxia. These results underscore how MR-based assessment of renal oxygenation by  $T_2^*, T_2$  is crucially dependent on monitoring accompanying changes in KS.

Furosemide has long been used in the clinic to increase urine flow rate and sodium excretion, and a furosemide “stress test” is suggested to predict renal

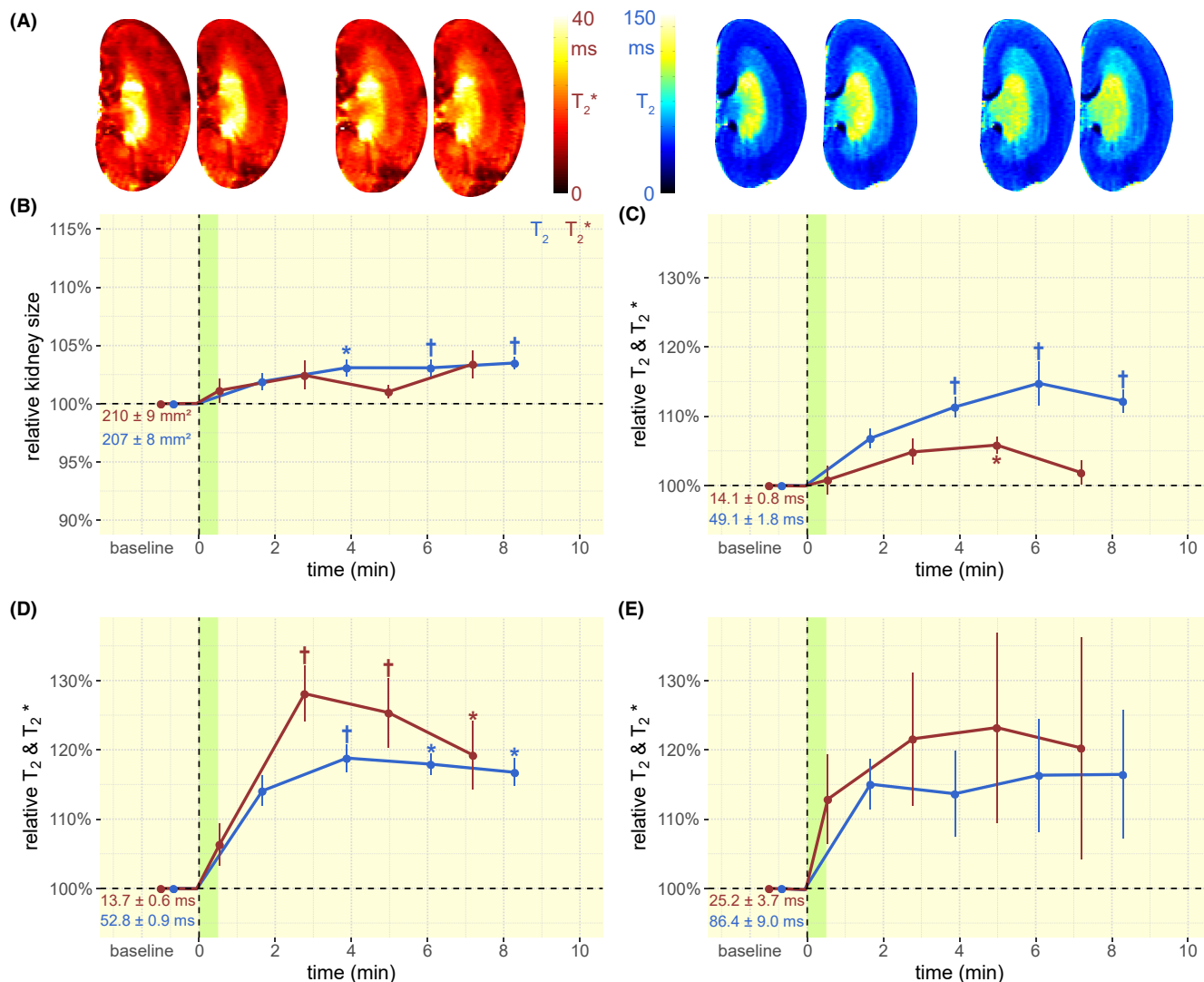


**FIGURE 6** Time courses following administration of furosemide. (A) Exemplary  $T_2, T_2^*$  maps obtained for a rat kidney in vivo. Time course of relative changes for (B) kidney size and  $T_2, T_2^*$  for (C) CO, (D) OM, and (E) IM. Colors, absolute baseline values, and significance signs as in Figure 1.

**TABLE 2** Ratio of  $(1 - \text{Sat})_{\text{occlusion}} / (1 - \text{Sat})_{\text{before occlusion}}$  obtained by the biophysical model for the three vascular occlusions (two consecutive  $T_2^*$  scans per occlusion)

$\frac{1 - \text{Sat}}{1 - \text{Sat}_0}$	Cortex	Outer medulla	Inner medulla
Aortic occlusion scan 1	$2.15 \pm 0.24$	$2.06 \pm 0.13$	$2.35 \pm 0.28$
Aortic occlusion scan 2	$2.25 \pm 0.29$	$2.10 \pm 0.14$	$2.32 \pm 0.33$
Venous occlusion scan 1	$2.30 \pm 0.15$	$2.23 \pm 0.08$	$2.16 \pm 0.19$
Venous occlusion scan 2	$2.29 \pm 0.16$	$1.89 \pm 0.11$	$2.90 \pm 0.28$
Combined occlusion scan 1	$2.01 \pm 0.13$	$2.20 \pm 0.09$	$1.91 \pm 0.10$
Combined occlusion scan 2	$2.01 \pm 0.13$	$2.11 \pm 0.11$	$2.04 \pm 0.15$

disease progression.<sup>45,57</sup> Furosemide decreases resorption in the thick ascending limb of the loop of Henle, resulting in increased tissue  $pO_2$ , particularly in the OM,<sup>58</sup> with reported increases in  $T_2^*$ ,  $T_2$ .<sup>45,59</sup> While our present  $T_2^*$ ,  $T_2$  results agree with these studies, our observation of a small KS increase indicates that this is

not solely the result of improved oxygenation. Rather, the increased KS is likely due to increased tubular fluid volume in the distal nephron, resulting in a mild form of compartment syndrome, again illustrating how  $T_2^*$ ,  $T_2$  overestimates tissue oxygenation if not adjusted by KS assessments.

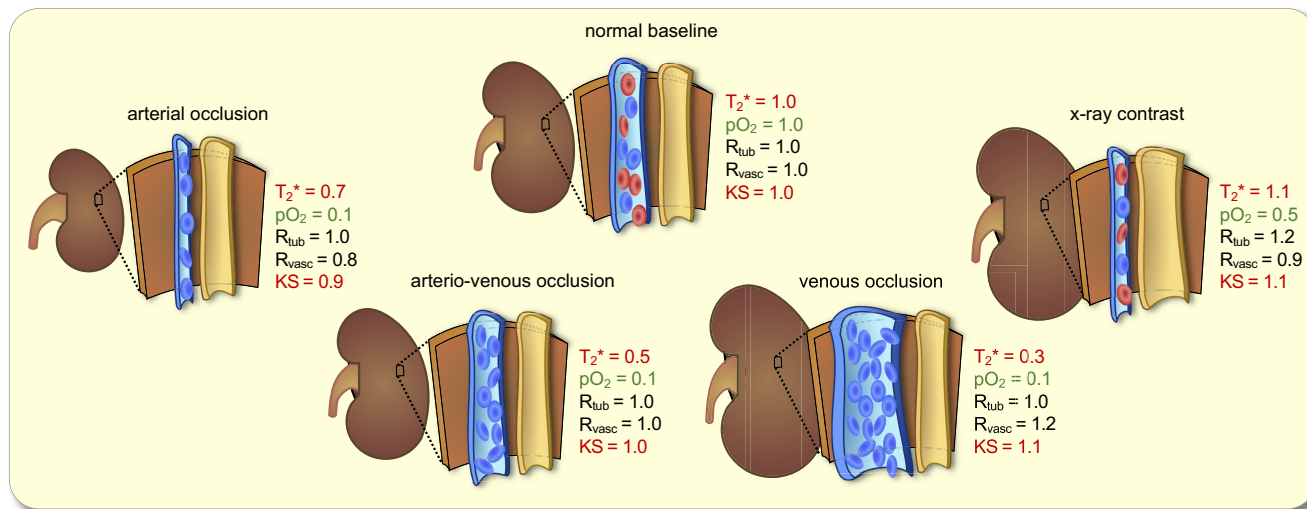


**FIGURE 7** Schematic overview delineating the qualitative relationship between kidney size and  $T_2^*$ .  $T_2^*$  mirrors the amount of deoxygenated hemoglobin per tissue volume (voxel) represented here by blue erythrocytes. The scheme depicts the tubular volume, represented by radius ( $R_{tub}$ ), the vascular volume represented by radius ( $R_{vasc}$ ), the average tissue  $pO_2$ , and the kidney size (KS) as well as their changes upon the acute interventions (not to scale). Changes in all parameters are expressed relative to normal baseline (arbitrarily defined as 1.0); approximate changes in tissue  $pO_2$  are derived from earlier studies.<sup>27,41,53,56</sup> Changes in renal  $T_2^*$  result from changes in intrarenal oxygenation (the balance between  $O_2$  delivery and  $O_2$  consumption) and in the intrarenal blood volume fraction. Aside from changes exerted by active vasomotion, changes in blood volume result from passive distension of vessels (as during renal venous occlusion), or from passive compression of vessels (as during aortic occlusion or the distension of the tubules following X-ray contrast). In cases where the blood volume fraction is changed,  $T_2^*$  changes do not correctly mirror changes in oxygenation, that is, in renal tissue  $pO_2$ . In acute scenarios such as occlusions and X-ray administration, changes in the vascular and tubular volume are often accompanied by changes in KS. Therefore, monitoring of changes in KS enables physiological interpretation of  $T_2^*$  as a measure of oxygenation.

Measurements of acute changes in KS alone can not differentiate between changes induced by renal blood volume versus tubular volume changes. However, this distinction will often be clear from the specific intervention performed in preclinical experiments, and will also be obvious in many clinical scenarios with acute KS changes. Furthermore, advanced MR methodology supports monitoring of acute changes in the tubular or in the blood volume fraction using diffusion-weighted imaging.<sup>60,61</sup>

The quantitative correction factors obtained for  $T_2^*$  and  $T_2$  (slope and intercept of the linear regressions with KS) for the specific interventions are only valid for the present experimental setting. Although similar qualitative relationships between acute changes in  $T_2^*$ ,  $T_2$  and KS will exist for comparable acute interventions in preclinical and clinical studies, specific quantitative correction factors will naturally depend on the particular experimental or clinical setting including the magnetic field strength, and species. Chronic kidney diseases, especially those with fibrotic alterations, will greatly affect the quantitative relationship between acute changes in  $T_2^*$ ,  $T_2$  and KS. Our calculations for the three vascular occlusions demonstrate that the changes in  $O_2$  saturation of Hb (Sat) can be extracted from measured changes in  $T_2^*$  and in kidney size by use of a biophysical model.

Our data showed a  $(1 - Sat)/(1 - Sat_0)$  ratio of  $\approx 2.1$ , averaged overall renal layers, all three occlusions, and over all occlusion time points, indicating a relative 2.1-fold increase in the proportion of deoxyHb. To the best of our knowledge, to date the literature reports only Sat data for the cortex, but not for the outer and inner medulla of rats. Estimates based on invasive near-infrared spectroscopy suggest a baseline cortical blood Sat of approximately 65%.<sup>53</sup> The average  $(1 - Sat)/(1 - Sat_0)$  ratio of 2.1 derived from our model calculations corresponds to a Sat decrease of about 60%. Assuming a baseline cortical Sat of 65%, the occlusion-induced Sat could be as low as 26%, which according to the oxyHb dissociation curve of rats, would be equivalent to a blood  $pO_2$  of about 22 mmHg.<sup>62</sup> This is consistent with tissue  $pO_2$  data we previously obtained using invasive probes. During aortic or venous occlusions, cortical tissue  $pO_2$  decreased by 80–90%, reaching values  $< 4$  mmHg.<sup>27,53</sup> This congruence indicates that the biophysical model yields physiologically plausible calibration ratios and Sat values.

The biophysical model facilitates quantitative assessment of relative changes in Sat from relative changes in renal  $T_2^*$  and KS. It provided physiologically plausible values for the specific setup used in our preclinical study as a mandatory precursor to clinical studies. Due to its non-invasive nature, our approach suits swift

translation from pre-clinical research to human studies. It is very much conceivable that MR-based estimates of relative changes in Sat may ultimately become a diagnostic biomarker. However, a number of prerequisites must be fulfilled to meet this goal. While our study obtained serial MR data in the same rats (intraindividual time courses) before the intervention (baseline) and during the acute intervention, this will be barely routine or practical in a typical clinical setting. To address this difference between our preclinical study and clinical reality, it is essential to obtain age, BMI, sex, and magnetic field strength corrected normal reference values for renal  $T_2^*$  and KS in healthy humans using standardized MRI protocols. A similar approach has been used for myocardial  $T_2^*$  mapping, which is now very well established for the quantitative assessment of tissue iron content and for the therapy of iron overload disorders.<sup>63–67</sup>

It stands to reason that the normal reference values of renal  $T_2^*$  and KS can be deduced from large population imaging studies such as the German National Cohort or the UKBiobank.<sup>68,69</sup> Using these standardized MR protocols in acute clinical scenarios, assessment of the deviation of the relationship between  $T_2^*$  and KS of individual patients or patient groups from the normal reference obtained for healthy subjects would allow quantitative estimation of alterations in  $O_2$  saturation of hemoglobin.

Our biophysical model assumes deoxyHb to be the dominating factor. This assumption applies very well to  $T_2^*$  which reflects the amount of deoxyHb per tissue volume. Its reciprocal value  $R_2^*$  is directly proportional to the fraction of deoxyHb ( $=1 - \text{Sat}$ ) and the blood volume fraction ( $= \text{blood volume}/\text{kidney volume}$ ).<sup>70</sup>  $T_2$  is a physical constant for perfused tissue. Its reciprocal value  $R_2$  scales linearly with blood oxygenation.<sup>71</sup>  $R_2$  includes contributions other than magnetic susceptibility. Modeling and calibration involved in converting  $T_2$  into Sat require further experimental studies.<sup>72</sup> This calibration should include renal  $T_2$  mapping during hyperoxia (100% inspiratory  $O_2$ ) to distinguish  $T_2$  contributions which are not related to magnetic susceptibility from those governed by the amount of deoxyHb per tissue volume.<sup>71</sup> Upon successful calibration of renal  $T_2$  versus Sat our biophysical model can be refined and applied for renal  $T_2$  oximetry, which will be our next target.

Previous studies showed that MR-based assessment of KS complements other markers for diagnosis and staging of kidney disorders. Here, we demonstrate that KS monitoring is essential for the physiological interpretation of acute changes in renal tissue oxygenation derived from  $T_2^*$ ,  $T_2$ . As KS can be readily obtained from  $T_2^*$ ,  $T_2$  maps without the need for additional scans, this should always accompany the assessment of MRI-derived oxygenation

results. Driven by technical advances including simultaneous  $T_2^*$  and  $T_2$  mapping,<sup>61,73</sup> renal MR oximetry can greatly support preclinical studies into the mechanisms of renal pathophysiology. Moreover, this non-invasive approach to probing renal oxygenation holds the promise of swift translation to human studies, for example, for the assessment of drug effects, and for clinically meaningful diagnosis. First steps toward this include adaptation of the MRI protocol for simultaneous KS and  $T_2^*$ ,  $T_2$  measurements, and reversible test interventions applicable to human beings.

## 4 | METHODS

### 4.1 | Animal preparation

Investigations were approved by the LaGeSo of Berlin in accordance with German Animal Protection Law and EU Directive 2010/63/EU. Male Wistar rats ( $n = 37$ , aged 12–13 weeks, 270–300 g, Harlan-Winkelmann, Borchon, Germany) were studied. An intraperitoneal dose of urethane (0.2 g/ml; 6 ml/kg, Sigma-Aldrich, Steinheim, Germany) was used as anesthesia throughout surgeries and MRI examinations. Urethane provides long-lasting anesthesia and has the least effects on cardiovascular and respiratory control compared to other anesthetics.<sup>49</sup> Preparation included insertion of vascular catheters and probes for measurements of hemodynamics and oxygenation.<sup>41,46,53,74</sup> In a subgroup ( $n = 13$ ), two MR-safe remotely controlled inflatable occluders were applied around the suprarenal aorta and the left renal vein.<sup>45–47</sup> Thereafter, rats were transferred into the MR scanner. They were spontaneously breathing and continuously provided with air (1 L/min). Body temperature was maintained at 37°. A balloon on the thorax was used for respiration-triggered MR data acquisition.<sup>45,46</sup>

### 4.2 | MRI experiments

MRI data were acquired on a 9.4 Tesla small animal MR system (Bruker Biospec 94/20, Bruker Biospin, Ettlingen, Germany) using a linear radiofrequency volume resonator and a 4-channel surface coil array tailored for rats (Bruker Biospin).<sup>37</sup> For geometrical planning and slice positioning,  $T_2$ -weighted pilot scans were acquired. Local volume selective magnetic field shimming was done on an ellipsoid accommodating the left kidney using an automatic optimization algorithm based on free induction decay length.  $T_2^*$  and  $T_2$  mapping were performed with respiration-gated protocols. Details of the MRI parameters are listed in [Table 3](#).

	<b>T<sub>2</sub>*-mapping</b>	<b>T<sub>2</sub>-mapping</b>
Method	Multi gradient-echo MRI	Multi spin-echo MRI
Repetition time TR (ms)	50	500
Number of echoes	10	13
First echo time TE <sub>1</sub> (ms)	2.1	6.4
Inter-echo time ΔTE (ms)	2.1	6.4
Excitation flip angle (°)	16	90
Number of averages NA	4	1
Acquisition time t <sub>acq.</sub> (s)	23	58
In-plane spatial resolution w/o zero filling (μm <sup>2</sup> )	226 × 445	
Field of view (mm <sup>2</sup> )	38.2 × 50.3	
Matrix size	169 × 113 (zero-filled to 169 × 215)	
Slice thickness (mm)	1.4	

**TABLE 3** Details of MRI protocols used for T<sub>2</sub>\* and T<sub>2</sub> mapping

### 4.3 | Image analysis

Parametric maps of absolute T<sub>2</sub>\* and T<sub>2</sub> were calculated by pixel-wise mono-exponential fitting to the signal intensities of the T<sub>2</sub>\*- and T<sub>2</sub>-weighted images acquired at different echo times.<sup>37</sup> Median T<sub>2</sub>\* and T<sub>2</sub> values for regions-of-interest (ROI) within the renal cortex (CO), outer medulla (OM), and inner medulla (IM) were calculated from the parameter maps. ROI placement was done with a standardized semi-automatic method, as previously described.<sup>75</sup> This procedure positions the ROIs (5 for CO and OM each, 3 for IM) such that they exclude the transition regions between renal layers to avoid partial volume effects. For T<sub>2</sub>\*, T<sub>2</sub> mapping-based determination of KS, segmentation of the coronal mid-slice cross-sectional area of the kidney (here referred to as “kidney size,” KS) was done using a previously described automatic bean-shaped model.<sup>37</sup>

### 4.4 | Longitudinal quantification of changes in kidney size and oxygenation upon pathophysiological interventions

To investigate the relationship between changes in T<sub>2</sub>\*, T<sub>2</sub> and KS, six pathophysiological interventions that alter renal tissue oxygenation reversibly (brief occlusion of the suprarenal aorta, the left renal vein or both; hypoxemia), and with longer-lasting effects (injection of CM or furosemide) were used. In addition to their effects on oxygenation, occlusion of the aorta results in decreased renal blood volume, occlusion of the renal vein induces an increase in renal blood volume, and simultaneous occlusion of both vessels does not affect renal blood volume. Administration of CM is expected to increase the tubular volume fraction concomitant with its effect on oxygenation.

Rats equipped with vascular occluders underwent a series of interleaved T<sub>2</sub>\* and T<sub>2</sub> mappings (short: MR scans) prior to the occlusions (control period), during occlusions, and following the release of occlusions. The aorta was occluded for 3.8 ± 0.3 min (*n* = 13 rats; time depending on respiration gating). The occluder was then deflated, and the animals were allowed to recover for at least 7 min to ensure complete restoration of pre-occlusion hemodynamics and oxygenation. Time of flight-based MR angiography was performed immediately after inflation/deflation of the occluder to confirm occlusion/reperfusion of the vessels.<sup>45–47</sup> After recovery from the aortic occlusion, the same procedure was performed for renal venous occlusion (*n* = 12), and subsequently for simultaneous combined aortic and venous occlusion (*n* = 10).

In the second subgroup (*n* = 11), rats underwent MR scans during a control period of normoxia with an FiO<sub>2</sub> of 21%, during a short period (3.8 ± 0.1 min) of hypoxia (FiO<sub>2</sub> = 10%) and 10 min of recovery (FiO<sub>2</sub> = 21%). The FiO<sub>2</sub> was monitored as previously described.<sup>45,48</sup>

In the third subgroup (*n* = 8), rats underwent MR scans before (control) and following a 1.5 ml bolus of iodixanol solution (320 mg/ml iodine, GE Healthcare Buchler, Braunschweig, Germany) injected into the thoracic aorta, followed by 0.2 ml saline chaser, as previously described.<sup>40,41</sup>

In the fourth subgroup (*n* = 5), rats underwent MR scans before (control) and following an i.v. bolus of furosemide (5 mg/kg, ratiopharm GmbH, Ulm, Germany) followed by a 0.2 ml saline chaser.

### 4.5 | Statistical analysis

Data were evaluated for Gaussian distribution using the Shapiro–Wilk test. Relative intervention-mediated

changes in KS and  $T_2^*$ ,  $T_2$  were analyzed using the non-parametric repeated-measures Friedman test, followed by Dunn's post hoc test with the Benjamini-Hochberg correction for multiple comparisons. Correlations between relative changes in KS and  $T_2^*$ ,  $T_2$  were assessed using repeated-measures correlation.<sup>76</sup> Data were analyzed using R v.3.6.3 with the packages "rstatix," "dunn.test," and "rmcorr."<sup>77-79</sup>  $p < 0.05$  was considered significant.

#### 4.6 | Biophysical model

To evaluate the quantitative features of the observed  $T_2^*$ -based signal changes and the relative changes in KS, we used a model to extract changes in  $O_2$  saturation of Hb (Sat) from measured changes in  $T_2^*$  and in KS for the three interventions involving vascular occlusions.

$T_2^*$  reflects the amount of deoxygenated Hb per tissue volume. Its reciprocal value  $R_2^*$  is proportional to the fraction of deoxygenated Hb ( $=1 - \text{Sat}$ ) and the blood volume fraction ( $BVF = \text{blood volume [BV]}/\text{kidney volume [KV]}$ ).<sup>70</sup>

$$R_2^* \sim (1 - \text{Sat}) \frac{BV}{KV} \quad (1)$$

For the model, we assume that all changes in KV ( $\Delta KV$ ) during the vascular occlusions are caused by blood volume changes ( $\Delta BV$ ).

$$\Delta BV = \Delta KV \quad (2)$$

With this assumption, the ratio of  $R_2^*$  obtained during the occlusions versus  $R_2^*$  observed for baseline conditions ( $R_{20}^*$ ) prior to the occlusion can be expressed as:

$$\frac{R_2^*}{R_{20}^*} = \frac{(1 - \text{Sat})}{(1 - \text{Sat}_0)} \frac{KV_0}{BV_0} \frac{(BV_0 + \Delta KV)}{(KV_0 + \Delta KV)} \quad (3)$$

Rearranging the ratio of the deoxygenated Hb fractions and substituting changes in the blood volume fraction ( $BVF = BV/KV$ ) leads to:

$$\frac{1 - \text{Sat}}{1 - \text{Sat}_0} = \frac{R_2^*}{R_{20}^*} BVF_0 \frac{1 + \frac{\Delta KV}{KV_0}}{BVF_0 + \frac{\Delta KV}{KV_0}} \quad (4)$$

Equation (4) relates the  $R_2^*$  ratio to the ratio of the deoxygenated Hb fractions using the baseline blood volume fraction and the relative kidney volume change as correction factors.

Assuming (i) that the  $O_2$  saturation of Hb at baseline and the degree of its decrease during the occlusions do not differ among the three occlusions, and (ii) that the KV

changes are uniform across the kidney, we can estimate the baseline  $BVF_0$  for the three renal layers. This estimation permits the calibration of Equation (4) to convert  $R_2^*$  ratios to ratios of  $(1 - \text{Sat})$ .

We measured kidney size by planimetry of the mid-slice cross-sectional area ( $A$ ). We converted this into kidney volume under the assumption that changes in the third dimension are similar to changes in the two measured dimensions:

$$\frac{\Delta KV}{KV_0} = \left( \frac{\Delta A}{A_0} + 1 \right)^3 - 1 \quad (5)$$

The calibration was done by minimizing the variance of the resulting  $\frac{1 - \text{Sat}}{1 - \text{Sat}_0}$  on the average deviation among the three occlusions. The calculated calibration factors  $BVF_0$  were 0.268, 0.394, and 0.273 for CO, OM, and IM, respectively.

#### ACKNOWLEDGMENTS

This work was supported by the German Research Foundation, CRC 1365 "Renoprotection" (Gefördert durch die Deutsche Forschungsgemeinschaft [DFG], SFB 1365 "Renoprotection"). We thank P.B. Persson, A. Anger, B. Flemming (Charité Berlin), A. Pohlmann, J. Periquito, H. Reimann (Max-Delbrück-Center for Molecular Medicine in the Helmholtz Association, Berlin), and D. Grosenick (Physikalisch-Technische Bundesanstalt Berlin) for technical and other support. Open Access funding enabled and organized by Projekt DEAL.

#### CONFLICT OF INTEREST

All authors declare no competing interests.

#### ORCID

Thoralf Niendorf  <https://orcid.org/0000-0001-7584-6527>  
Erdmann Seeliger  <https://orcid.org/0000-0002-5685-8044>

#### REFERENCES

1. Levin A, Tonelli M, Bonventre J, et al. Global kidney health 2017 and beyond: a roadmap for closing gaps in care, research, and policy. *Lancet*. 2017;390:1888-1917.
2. Kellum JA, Ronco C, Bellomo R. Conceptual advances and evolving terminology in acute kidney disease. *Nat Rev Nephrol*. 2021;17:493-502.
3. Pickkers P, Ostermann M, Joannidis M, et al. The intensive care medicine agenda on acute kidney injury. *Intensive Care Med*. 2017;43:1198-1209.
4. Fählng M, Seeliger E, Patzak A, Persson PB. Understanding and preventing contrast-induced acute kidney injury. *Nat Rev Nephrol*. 2017;13:169-180.
5. Molitoris BA. Urinary biomarkers: alone are they enough? *J Am Soc Nephrol*. 2015;26:1485-1488.

6. van Duijl TT, Soonawala D, de Fijter JW, Ruhaak LR, Cobbaert CM. Rational selection of a biomarker panel targeting unmet clinical needs in kidney injury. *Clin Proteomics*. 2021;18:10.
7. Porrini E, Ruggenti P, Luis-Lima S, et al. Estimated GFR: time for a critical appraisal. *Nat Rev Nephrol*. 2019;15:177-190.
8. van Duijl TT, Ruhaak LR, de Fijter JW, Cobbaert CM. Kidney injury biomarkers in an academic hospital setting: where are we now? *Clin Biochem Rev*. 2019;40:79-97.
9. Niendorf T, Pohlmann A, Arakelyan K, et al. How bold is blood oxygenation-dependent (BOLD) magnetic resonance imaging of the kidney? Opportunities, challenges and future directions. *Acta Physiol (Oxf)*. 2015;213:19-38.
10. Matejovic M, Ince C, Chawla LS, et al. Renal hemodynamics in AKI: in search of new treatment targets. *J Am Soc Nephrol*. 2016;27:49-58.
11. Selby NM, Blankestijn PJ, Boor P, et al. Magnetic resonance imaging biomarkers for chronic kidney disease: a position paper from the European Cooperation in Science and Technology Action PARENCHIMA. *Nephrol Dial Transplant*. 2018;33:ii4-ii14.
12. Caroli A, Remuzzi A, Remuzzi G. Does MRI trump pathology? A new era for staging and monitoring of kidney fibrosis. *Kidney Int*. 2020;97:442-444.
13. Simms R, Sourbron S. Recent findings on the clinical utility of renal magnetic resonance imaging biomarkers. *Nephrol Dial Transplant*. 2020;35:915-919.
14. Puelles VG, Combes AN, Bertram JF. Clearly imaging and quantifying the kidney in 3D. *Kidney Int*. 2021;100:780-786.
15. Charlton JR, Xu Y, Wu T, et al. Magnetic resonance imaging accurately tracks kidney pathology and heterogeneity in the transition from acute kidney injury to chronic kidney disease. *Kidney Int*. 2021;99:173-185.
16. Selby NM, Duranteau J. New imaging techniques in AKI. *Curr Opin Crit Care*. 2020;26:543-548.
17. Caroli A, Remuzzi A, Lerman LO. Basic principles and new advances in kidney imaging. *Kidney Int*. 2021;100:1001-1011.
18. Bane O, Mendichovszky IA, Milani B, et al. Consensus-based technical recommendations for clinical translation of renal BOLD MRI. *MAGMA*. 2020;33:199-215.
19. Li LP, Hack B, Seeliger E, Prasad PV. MRI mapping of the blood oxygenation sensitive parameter T(2)\* in the kidney: basic concept. *Methods Mol Biol*. 2021;2216:171-185.
20. Pohlmann A, Back SJ, Fekete A, et al. Recommendations for preclinical renal MRI: a comprehensive open-access protocol collection to improve training, reproducibility, and comparability of studies. *Methods Mol Biol*. 2021;2216:3-23.
21. Buchanan CE, Mahmoud H, Cox EF, et al. Quantitative assessment of renal structural and functional changes in chronic kidney disease using multi-parametric magnetic resonance imaging. *Nephrol Dial Transplant*. 2020;35:955-964.
22. Gooding KM, Lienczewski C, Papale M, et al. Prognostic imaging biomarkers for diabetic kidney disease (iBEAT): study protocol. *BMC Nephrol*. 2020;21:242.
23. Magistroni R, Corsi C, Martí T, Torra R. A review of the imaging techniques for measuring kidney and cyst volume in establishing autosomal dominant polycystic kidney disease progression. *Am J Nephrol*. 2018;48:67-78.
24. Lee SP, Silva AC, Ugurbil K, Kim SG. Diffusion-weighted spin-echo fMRI at 9.4 T: microvascular/tissue contribution to BOLD signal changes. *Magn Reson Med*. 1999;42:919-928.
25. Han S, Son JP, Cho H, Park JY, Kim SG. Gradient-echo and spin-echo blood oxygenation level-dependent functional MRI at ultrahigh fields of 9.4 and 15.2 Tesla. *Magn Reson Med*. 2019;81:1237-1246.
26. Prasad PV. Update on renal blood oxygenation level-dependent MRI to assess intrarenal oxygenation in chronic kidney disease. *Kidney Int*. 2018;93:778-780.
27. Pohlmann A, Arakelyan K, Hentschel J, et al. Detailing the relation between renal T2\* and renal tissue pO2 using an integrated approach of parametric magnetic resonance imaging and invasive physiological measurements. *Invest Radiol*. 2014;49:547-560.
28. Niendorf T, Seeliger E, Cantow K, Flemming B, Waiczies S, Pohlmann A. Probing renal blood volume with magnetic resonance imaging. *Acta Physiol (Oxf)*. 2020;228:e13435.
29. Brezis M, Rosen S. Hypoxia of the renal medulla—its implications for disease. *N Engl J Med*. 1995;332:647-655.
30. Evans RG, Ince C, Joles JA, et al. Haemodynamic influences on kidney oxygenation: the clinical implications of integrative physiology. *Clin Exp Pharmacol Physiol*. 2013;40:106-122.
31. Seeliger E, Sendeski M, Rihal CS, Persson PB. Contrast-induced kidney injury: mechanisms, risk factors, and prevention. *Eur Heart J*. 2012;33:2007-2015.
32. Shu S, Wang Y, Zheng M, et al. Hypoxia and hypoxia-inducible factors in kidney injury and repair. *Cell*. 2019;8:207-228.
33. Hultstrom M, Becirovic-Agic M, Jonsson S. Comparison of acute kidney injury of different etiology reveals in-common mechanisms of tissue damage. *Physiol Genomics*. 2018;50:127-141.
34. Ma S, Evans RG, Iguchi N, et al. Sepsis-induced acute kidney injury: a disease of the microcirculation. *Microcirculation*. 2019;26:e12483.
35. Jensen AM, Norregaard R, Topcu SO, Frokiaer J, Pedersen M. Oxygen tension correlates with regional blood flow in obstructed rat kidney. *J Exp Biol*. 2009;212:3156-3163.
36. Scholz H, Boivin FJ, Schmidt-Ott KM, et al. Kidney physiology and susceptibility to acute kidney injury: implications for renoprotection. *Nat Rev Nephrol*. 2021;17:335-349.
37. Gladysz T, Millward JM, Cantow K, et al. Reliable kidney size determination by magnetic resonance imaging in pathophysiological settings. *Acta Physiol (Oxf)*. 2021;233:e13701.
38. Gottschalk CW, Mylle M. Micropuncture study of pressures in proximal tubules and peritubular capillaries of the rat kidney and their relation to ureteral and renal venous pressures. *Am J Physiol*. 1956;185:430-439.
39. Ueda J, Nygren A, Hansell P, Ulfendahl HR. Effect of intravenous contrast media on proximal and distal tubular hydrostatic pressure in the rat kidney. *Acta Radiol*. 1993;34:83-87.
40. Seeliger E, Becker K, Ladwig M, Wronski T, Persson PB, Flemming B. Up to 50-fold increase in urine viscosity with iso-osmolar contrast media in the rat. *Radiology*. 2010;256:406-414.
41. Seeliger E, Cantow K, Arakelyan K, Ladwig M, Persson PB, Flemming B. Low-dose nitrite alleviates early effects of an X-ray contrast medium on renal hemodynamics and oxygenation in rats. *Invest Radiol*. 2014;49:70-77.
42. Cruces P, Lillo P, Salas C, et al. Renal decapsulation prevents intrinsic renal compartment syndrome in ischemia-reperfusion-induced acute kidney injury: a physiologic approach. *Crit Care Med*. 2018;46:216-222.

43. Evans RG. Renal decapsulation to treat ischemic acute kidney injury: a new twist in an old tale. *Crit Care Med*. 2018;46:332-333.
44. Herrler T, Tischer A, Meyer A, et al. The intrinsic renal compartment syndrome: new perspectives in kidney transplantation. *Transplantation*. 2010;89:40-46.
45. Cantow K, Ladwig-Wiegard M, Flemming B, Fekete A, Hosszu A, Seeliger E. Reversible (patho)physiologically relevant test interventions: rationale and examples. *Methods Mol Biol*. 2021;2216:57-73.
46. Cantow K, Ladwig-Wiegard M, Flemming B, Pohlmann A, Niendorf T, Seeliger E. Monitoring renal hemodynamics and oxygenation by invasive probes: experimental protocol. *Methods Mol Biol*. 2021;2216:327-347.
47. Pohlmann A, Cantow K, Huelnhagen T, et al. Experimental MRI monitoring of renal blood volume fraction variations en route to renal magnetic resonance oximetry. *Tomography*. 2017;3:188-200.
48. Cantow K, Pohlmann A, Flemming B, et al. Acute effects of ferumoxytol on regulation of renal hemodynamics and oxygenation. *Sci Rep*. 2016;20:29965. doi:10.1038/srep29965
49. Kaucsar T, Hosszu A, Seeliger E, Reimann HM, Fekete A. Preparation and monitoring of small animals in renal MRI. *Methods Mol Biol*. 2021;2216:45-55.
50. Hesp AC, Schaub JA, Prasad PV, et al. The role of renal hypoxia in the pathogenesis of diabetic kidney disease: a promising target for newer renoprotective agents including SGLT2 inhibitors? *Kidney Int*. 2020;98:579-589.
51. Cao J, Zhu S, Ye M, et al. Comparison of renal artery vs renal artery-vein clamping during partial nephrectomy: a system review and meta-analysis. *J Endourol*. 2020;34:523-530.
52. Jongkind V, Yeung KK, Akkersdijk GJ, et al. Juxtarenal aortic aneurysm repair. *J Vasc Surg*. 2010;52:760-767.
53. Grosenick D, Cantow K, Arakelyan K, et al. Detailing renal hemodynamics and oxygenation in rats by a combined near-infrared spectroscopy and invasive probe approach. *Biomed Opt Express*. 2015;6:309-323.
54. Lankadeva YR, May CN, Cochrane AD, et al. Influence of blood haemoglobin concentration on renal haemodynamics and oxygenation during experimental cardiopulmonary bypass in sheep. *Acta Physiol (Oxf)*. 2021;231:e13583.
55. Seeliger E, Flemming B, Wronski T, et al. Viscosity of contrast media perturbs renal hemodynamics. *J Am Soc Nephrol*. 2007;18:2912-2920.
56. Arakelyan K, Cantow K, Hentschel J, et al. Early effects of an x-ray contrast medium on renal T(2)\*/T(2) MRI as compared to short-term hyperoxia, hypoxia and aortic occlusion in rats. *Acta Physiol (Oxf)*. 2013;208:202-213.
57. McMahon BA, Chawla LS. The furosemide stress test: current use and future potential. *Ren Fail*. 2021;43:830-839.
58. Brezis M, Agmon Y, Epstein FH. Determinants of intrarenal oxygenation. I. Effects of diuretics. *Am J Physiol*. 1994;267:F1059-F1062.
59. Warner L, Glockner JF, Woollard J, Textor SC, Romero JC, Lerman LO. Determinations of renal cortical and medullary oxygenation using blood oxygen level-dependent magnetic resonance imaging and selective diuretics. *Invest Radiol*. 2011;46:41-47.
60. van der Bel R, Gurney-Champion OJ, Froeling M, Stroes ESG, Nederveen AJ, Krediet CTP. A tri-exponential model for intravoxel incoherent motion analysis of the human kidney: In silico and during pharmacological renal perfusion modulation. *Eur J Radiol*. 2017;91:168-174.
61. Periquito JDS, Gladysz T, Millward JM, et al. Continuous diffusion spectrum computation for diffusion weighted magnetic resonance imaging of the kidney tubule system. *Quant Imaging Med Surg*. 2021;11:3098-3119.
62. Quatrini U, Licciardi A, Morici G. Oxygen-haemoglobin dissociation curve in hypoxic rats of first or second generation. *Clin Exp Pharmacol Physiol*. 1993;20:269-274.
63. Anderson LJ, Holden S, Davis B, et al. Cardiovascular T2-star (T2\*) magnetic resonance for the early diagnosis of myocardial iron overload. *Eur Heart J*. 2001;22:2171-2179.
64. Chu WC, Au WY, Lam WW. MRI of cardiac iron overload. *J Magn Reson Imaging*. 2012;36:1052-1059.
65. Roy C, Slimani A, de Meester C, et al. Age and sex corrected normal reference values of T1, T2 T2\* and ECV in healthy subjects at 3T CMR. *J Cardiovasc Magn Reson*. 2017;19:72.
66. Fernandes JL. MRI for iron overload in thalassemia. *Hematol Oncol Clin North Am*. 2018;32:277-295.
67. Hsu CC, Senussi NH, Fertrin KY, Kowdley KV. Iron overload disorders. *Hepatol Commun*. 2022;6:1842-1854.
68. Bamberg F, Kauczor HU, Weckbach S, et al. Whole-body mr imaging in the German national cohort: rationale, design, and technical background. *Radiology*. 2015;277:206-220.
69. Schuppert C, Krüchten RV, Hirsch JG, et al. Whole-body magnetic resonance imaging in the large population-based german national cohort study: predictive capability of automated image quality assessment for protocol repetitions. *Invest Radiol*. 2022;57:478-487.
70. Ogawa S, Menon RS, Tank DW, et al. Functional brain mapping by blood oxygenation level-dependent contrast magnetic resonance imaging. A comparison of signal characteristics with a biophysical model. *Biophys J*. 1993;64:803-812.
71. van Zijl PC, Eleff SM, Ulatowski JA, et al. Quantitative assessment of blood flow, blood volume and blood oxygenation effects in functional magnetic resonance imaging. *Nat Med*. 1998;4:159-167.
72. Li W, Xu F, Zhu D, van Zijl PCM, Qin Q. T(2)-oximetry-based cerebral venous oxygenation mapping using Fourier-transform-based velocity-selective pulse trains. *Magn Reson Med*. 2022;88:1292-1302.
73. Herrmann CJJ, Els A, Boehmert L, et al. Simultaneous T2 and T 2 \* mapping of multiple sclerosis lesions with radial RARE-EPI. *Magn Reson Med*. 2021;86:1383-1402.
74. Cantow K, Evans RG, Grosenick D, et al. Quantitative assessment of renal perfusion and oxygenation by invasive probes: basic concepts. *Methods Mol Biol*. 2021;2216:89-107.
75. Riazzy L, Milani B, Periquito JS, et al. Subsegmentation of the kidney in experimental MR images using morphology-based regions-of-interest or multiple-layer concentric objects. *Methods Mol Biol*. 2021;2216:549-564.
76. Bakdash JZ, Marusich LR. Repeated measures correlation. *Front Psychol*. 2017;8:456.
77. Bakdash JZ, Marusich LR. rmcrr: repeated measures correlation. R package version 043. 2021.
78. Dinno A. dunn.test: Dunn's Test of Multiple Comparisons Using Rank Sums. R package version 1.3.5. 2017.

79. Kassambara A. rstatix: Pipe-Friendly Framework for Basic Statistical Tests. R package version 0.7.0. 2021.

### SUPPORTING INFORMATION

Additional supporting information can be found online in the Supporting Information section at the end of this article.

**How to cite this article:** Cantow K, Gladytz T, Millward JM, Waiczies S, Niendorf T, Seeliger E. Monitoring kidney size to interpret MRI-based assessment of renal oxygenation in acute pathophysiological scenarios. *Acta Physiol.* 2023;237:e13868. doi: [10.1111/apha.13868](https://doi.org/10.1111/apha.13868)